ACS OMEGA

http://pubs.acs.org/journal/acsodf

Article

Utilization of Biomass Fly Ash for Improving Quality of Organic Dye-Contaminated Water

Safana Dogar, Sana Nayab, Muhammad Qamar Farooq, Amir Said, Raheel Kamran, Hatice Duran,* and Basit Yameen*

Cite This: *ACS Omega* 2020, 5, 15850−15864

Read Online

ACCESS | Metrics & More | Article Recommendations | Supporting Information

ABSTRACT: Development of innovative methodologies to convert biomass ash into useful materials is essential to sustain the growing use of biomass for energy production. Herein, a simple chemical modification approach is employed to functionalize biomass fly ash (BFA) with 3-aminopropyltriethoxy silane (APTES) to develop an inexpensive and efficient adsorbent for water remediation. The amine-functionalized BFA (BFA−APTES) was fully characterized by employing a range of characterization techniques. Adsorption behavior of BFA−APTES was evaluated against two anionic dyes, namely, alizarin red S (ARS) and bromothymol blue (BTB). In the course of experimental data analysis, the computation tools of data fitting for linear and nonlinear form of Langmuir, Freundlich, and the modified Langmuir−Freundlich adsorption isotherms were used with the aid of Matlab R2019b. In order to highlight the misuse of linearization of adsorption models, the sum of the squares of residues (SSE) values obtained from nonlinear models are compared with R^2 values obtained from the linear regression. The accuracy of the data fitting was checked by the use of SSE as an error function instead of the coefficient of determination, R^2. The dye adsorption capacity of BFA−APTES was also compared with the nonfunctionalized BFA. The maximum adsorption capacities of BFA−APTES for ARS and BTB dye molecules were calculated to be around 13.42 and 15.44 mg/g, respectively. This value is approximately 2−3 times higher than the pristine BFA. A reasonable agreement between the calculated and experimental values of q_e obtained from the nonlinear form of kinetic models verified the importance of using equations in their original form. The experimentally calculated thermodynamic parameters including molar standard Gibbs free energy ($\Delta_{ad}G^0_m$) and molar standard enthalpy change ($\Delta_{ad}H^0_m$) reflected that the process of adsorption of dye molecules on the BFA−APTES adsorbent was spontaneous and exothermic in nature. Moreover, the used BFA−APTES adsorbent could be regenerated and reused for several cycles with significant dye adsorption capacity. The remediation capability of the BFA−APTES adsorbent against ARS dye was also demonstrated by packing a small column filled with the BFA−APTES adsorbent and passing a solution of ARS through it. Overall, we provide a simple and scalable route to convert BFA into an efficient adsorbent for water remediation applications.

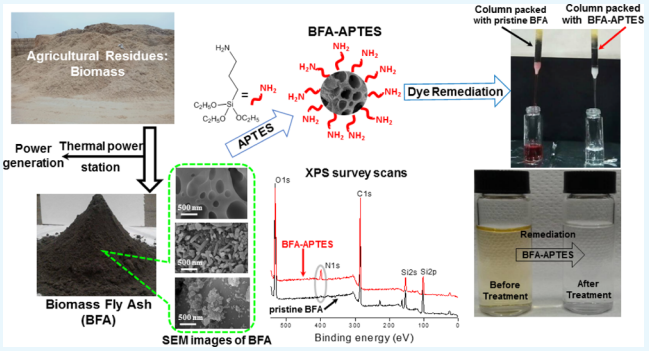

1. INTRODUCTION

Human population has increased by more than 50% in the past 5 decades, and according to an estimate by World Population Clock, there are about 7.78 billion humans living on planet Earth as of May 2020. Increase in population increases the demand of resources that are necessary to sustain the ever-improving standard of living. Besides increase in the demand of several other resources, energy demand is on a continuous rise. Electricity constitutes an important part of the global energy demand. According to International Energy Agency (IEA), the total gross electricity production was 26,700 TWh in 2018, which is about 3.8% higher than gross energy production during 2017. Despite much debated negative environmental effects associated with the use of coal, it is still the largest contributor to the global electricity generation. Recently, plant biomass is gaining popularity as the thermal source of electricity because of its low cost and availability in large quantities particularly as agricultural residues. In addition, the plant biomass is considered as a renewable and carbon neutral source of electricity because the CO_2 produced during the combustion of plant biomass in thermal power stations can be reused by the plants in the process of photosynthesis to generate more biomass.[1,2]

Received: February 28, 2020
Accepted: June 4, 2020
Published: June 22, 2020

https://dx.doi.org/10.1021/acsomega.0c00889
ACS Omega 2020, 5, 15850−15864

Combustion of coal and biomass in thermal power stations results in the generation of huge amounts of ash residues. It has been conservatively estimated that about 750 million tons of coal ash and about 480 million tons of biomass ash are globally produced every year.[3−8] Major portion of these ash residues ends up in landfills with a potential of inflicting serious environmental risks. Finding recycling technologies to mitigate the environmental impacts of ash residues is a formidable challenge and an interesting opportunity at the same time. With the widespread use of coal as the fuel in thermal power stations, bulk of the research work on management and utilization of ash residues is focused on the ash produced from the combustion of coal. The ash residues produced during the combustion of coal and biomass show markedly different physiochemical natures. Coal ash generally consists of spherical-shaped particles. The chemical composition of coal fly ash depends on the type of coal (bituminous, subbituminous, or lignite) used during the combustion process. Based on the chemical composition of the coal ash, the American Society of Testing and Material (ASTM C618) categorizes the coal ash residues into two main classes: Class F and Class C. In the case of Class F ash residues, the combined SiO_2, Fe_2O_3, and Al_2O_3 contents constitute >70%, and these residues are low in lime content. The SiO_2, Fe_2O_3, and Al_2O_3 contents of Class C ash residues are between 50 and 70%, and these residues are rich in lime content.[9] On the other hand, the biomass ash residues are generally classified as fly ash and bottom ash. The fly ash consists of fine particles that rise with the flue gases, while the bottom ash consists of relative larger particles and are collected at the bottom of the furnace. Both types of biomass ash residues consist of irregular-shaped particles. SiO_2 is the major component of the bottom ash along with the varying concentrations of other constituents including Al_2O_3, Fe_2O_3, CaO, K_2O, Na_2O, and MgO. Fly ash on the other hand can consist of large percentages of plant nutrients including K along with the constituents found in the bottom ash. The chemical composition of fly ash residues shows relatively larger variations in its chemical constituents. The variations in chemical compositions of fly ash residues stem from the fact that biomass thermal power station can use a mixture of different types of agricultural biomasses (e.g., wheat straw, rice husk, and corn stakes to name a few) with different percentage contributions of each type in the actual feed.[8,10]

With the growing understanding of the physiochemical natures of the ash residues, the scientific community across the world is investing serious efforts in finding new avenues for recycling of ash residues. Because of their pozzolanic and cementitious properties, coal ash residues have become an attractive material for cement and construction industry. Recent efforts for expanding the application profile of coal fly ash have revealed the potential of coal fly ash residues as functional materials for application in environmental remediation and catalysis. Several studies are available that highlight the efficiency of coal fly ash and materials derived from it (e.g., organocomposites and porous materials including zeolites, mesoporous silica) as adsorbents for removal of dyes, toxic metal ions, radioactive pollutants, organic pollutants such as benzene, toluene, and *o*- and *p*-xylene, gaseous pollutants such as CO_2, H_2S, and SO_2 as well as support material for catalysts, photocatalysts, and electrocatalysts.[6,11−20] Because of their distinct chemical nature, biomass ash residues do not show pozzolanic and cementitious properties; however, the potential of biomass ash as part of cement mortar[21−26] is widely investigated. Besides, the potential of biomass fly ash (BFA) for other applications is also being explored. Reports from Guo et al. and Rafael López et al. have recently demonstrated the potential of BFA for capturing of CO_2.[27,28] In a related effort, Fernández-Delgado Juárez et al. successfully applied wood ash for removal of CO_2 and H_2S and purification of biogas.[29] In another study, BFA was applied as the adsorbent to remove lignin from effluents generated during the kraft pulping process. The fly ash adsorbent was also found to reduce the chemical oxygen demand and turbidity of effluents.[30] In the same vein, Novais et al. have demonstrated the efficiency of BFA-derived geopolymer spheres and monoliths for removal of methylene blue from aqueous solutions.[31,32]

It is worth mentioning here that majority of the reported work do not consider rationally controlling the surface chemical properties of ash residues to modulate their remediation properties. In the context of application of BFA for capturing of CO_2, attempts have been made to introduce amine groups by the simple wet impregnation method.[33,34] The wet impregnation method is a convenient way of introducing certain functional groups in ash residues; however, the application of materials developed through this method is limited to capturing of gaseous pollutants. Surface chemical properties of materials can be conveniently and robustly controlled by anchoring appropriate organosilanes on their surface, a process designated as silanization.[35−37] In some studies, organosilanes have been applied to modify the surface chemical nature of coal fly ash for their better integration as fillers in composite materials.[38−40] However, to the best of our knowledge, no attempts have been made to apply the process of silanization for imparting specific functional group on the surface of BFA and apply them for remediation of dye-contaminated aqueous solutions. Herein, we report a convenient silanization method for anchoring amine groups on the surface of BFA by using 3-aminopropyltriethoxysilane (APTES). The resulting amine-functionalized BFA was applied as the adsorbent for remediation of dye-contaminated water solutions. The remediation characteristics of amine-functionalized fly ash were compared with the pristine fly ash. Special attention is given to emphasize the importance of application of isotherm models in the nonlinear form and correct statistical method (usage of SSE instead of R^2) as a corrective measure for adsorption studies because linearization may cause malpractice.

2. RESULTS AND DISCUSSION

Scheme 1 depicts the surface chemistry of BFA surface functionalization during activation and APTES modification. According to BET analysis, the specific surface areas of the A-

Scheme 1. Schematic Illustration of the Surface Functionalization of BFA with APTES

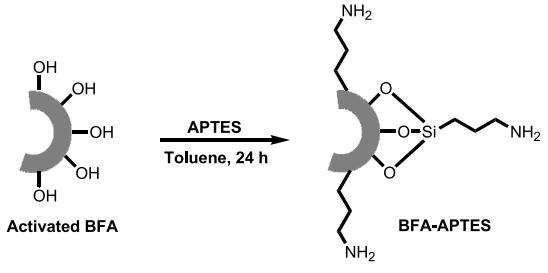

https://dx.doi.org/10.1021/acsomega.0c00889
ACS Omega 2020, 5, 15850−15864

BFA and BFA−APTES were calculated to be 95.72 and 8.15 $m^2 g^{-1}$, while pore volumes were 0.071 and 0.015 $cm^3 g^{-1}$ and pore diameters were 1.697 and 1.061 nm, respectively.

The scanning electron microscopy (SEM) imaging was used to reveal the morphology of A-BFA before and after functionalization with APTES (Figure 1). A-BFA and BFA−APTES displayed heterogeneous surface characteristics with macropores (diameter >50 nm) and particles with a range of different sizes (from 20 to 500 nm) and morphologies. Even some of the particles were found to be mesoporous in nature. Micropore size was not affected by surface treatment (Figure 1a,d), while there was almost one order of magnitude decrease in the particle size (Figure 1c,f). This drastic reduction in particle size may influence the kinetic parameters of adsorption.[41]

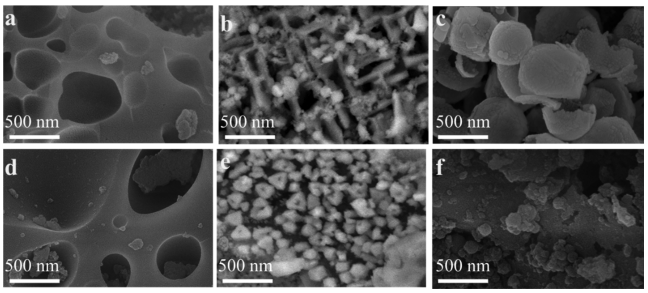

Figure 1. SEM images revealing particles of variety of different sizes and morphologies in A-BFA (a−c) and BFA−APTES (d−f).

The surface chemical composition of A-BFA before and after silanization was monitored by X-ray photoelectron spectroscopy (XPS) analysis (Figure 2). The survey scan of A-BFA and BFA−APTES showed signals at 150 and 100 eV, which correspond to the binding energies of Si 2s and Si 2p orbitals of the Si component of BFA. The signals for the C 1s and O 1s orbitals of the carbon and oxygen contents of A-BFA and BFA−APTES were evidenced by the signals at 284 and 530 eV. The C 1s signal in the survey scan of A-BFA can be attributed to the unburnt carbon component of BFA. The appearance of the N 1s orbital signal at 400 eV in the XPS survey scan of BFA−APTES validated the functionalization of BFA with APTES. The survey scan of A-BFA did not show any signal for nitrogen, confirming that the N 1s signal in the survey scan of BFA−APTES is originating from the amino groups decorated on the surface of BFA during the process of silanization with APTES.

Thermogravimetric analysis (TGA) was performed to quantify the extent of surface functionalization of A-BFA with APTES (Figure 3). Both ash residues were dried in an oven before subjecting to TGA. The 7.2% total weight loss observed in the case of A-BFA can be attributed to the loss of any absorbed water molecules and the unburnt carbon content of A-BFA. The TGA thermogram of BFA−APTES showed a total weight loss of 9.4%, which is 2.2% higher than the weight loss observed in the case of A-BFA. The additional weight loss observed in the case of BFA−APTES can be considered as the amount of APTES functionalized on the surface of A-BFA. From this analysis, it can be inferred that every 100 g of the BFA−APTES sample contains 2.2 g of APTES functionality in it. Furthermore, it can be concluded that each portion of 100 g of BFA−APTES offers 0.033 moles of $-NH_2$ groups. The percentage weight loss after functionalization with silane monolayers is generally in the range of 1−2 wt %. Comparing with our previously reported work,[42,43] the weight loss of 2.2 wt % observed in this study is reasonably reliable. Combining TGA and BET (8.15 m^2/g) data suggests that 2.7 mg (1.22×10^{-5} mole) of APTES is spread per m^2 of the adsorbent, which translates into 7.35×10^{18} molecules of APTES grafted per m^2 of BFA−APTES.

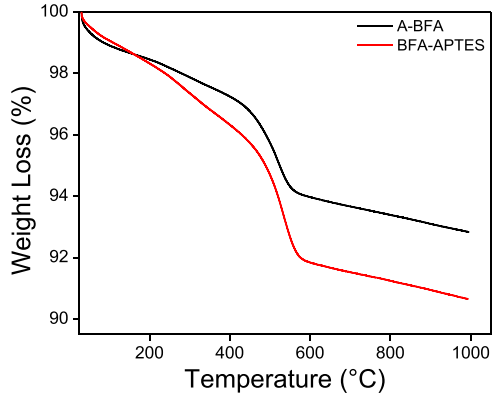

Figure 3. TGA of A-BFA and APTES-functionalized BFA (BFA−APTES).

After successful functionalization of BFA with APTES, supported by the XPS surface chemical analysis and TGA, the adsorption properties of A-BFA and BFA−APTES were investigated against two anionic dyes, namely, alizarin red S (ARS) and bromothymol blue (BTB) (Figure 4). ARS,

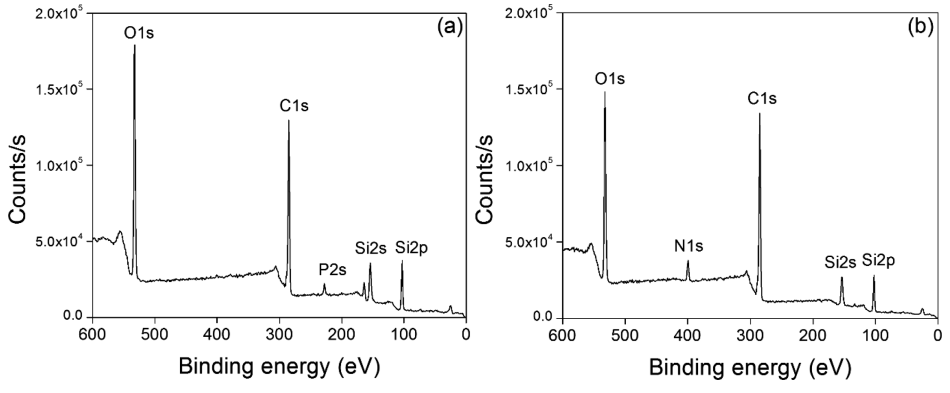

Figure 2. XPS survey scans of (a) A-BFA and (b) APTES-functionalized BFA.

https://dx.doi.org/10.1021/acsomega.0c00889
ACS Omega 2020, 5, 15850−15864

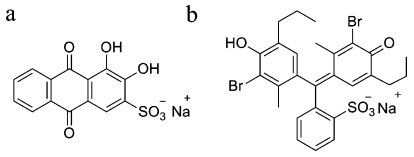

Figure 4. Chemical structures of anionic dyes: (a) ARS (b) BTB.

anthraquinone dye, is used as a staining agent in textile industries.[44] In addition, this dye is also used to stain biological specimens, such as mineralized bones in vertebrate groups and small invertebrate embryos.[45] ARS cannot be completely degraded by general chemical, physical, and biological processes.[46] This resistance to degradation is attributed to the complex structures of the aromatic rings that afford high physicochemical, thermal, and optical stability.[47] BTB, a triphenylmethane dye, is also frequently used for dyeing in the textile industry.[48] It has the potential of causing damage to lungs and mucous membranes.[49] Prolonged exposures to BTB-contaminated water may even lead to organ damage.[50] A review of the recent literature shows that BTB has been employed in the development of pH sensors as well.[51,52] These considerations laid the basis of our choice of ARS and BTB as model dye contaminants.

2.1. Effect of pH. The nature and magnitude of overall electrostatic charge on the interacting adsorbent and adsorbate system determine the capacity and efficiency of the process of remediation. In case of materials bearing functional groups (e.g., amines, carboxylic acid, sulfonic acid, phosphonic acid, or zwitterionic groups) that can undergo protonation or deportation, a change in the pH of the surrounding medium can lead to a change in the nature and magnitude of the electrostatic charge on the material.[53−55] Consequently, the change in pH of the medium can impact the capacity and efficiency of the process of remediation, which makes it necessary to evaluate the impact of pH of the medium on the capacity and efficiency of the process of remediation. The effect of pH on the adsorption capacity of A-BFA and BFA−APTES as adsorbent toward the employed dyes was determined by performing adsorption studies in the pH range of 2−12 (Figure 5). The pH of dye solutions was adjusted by using 0.1 M aqueous sodium hydroxide and 0.1 M aqueous hydrochloric acid solutions. Twenty milligrams of A-BFA and BFA−APTES adsorbents was separately added to 10 mL of dye solutions (15 ppm for ARS and 10 ppm for BTB) and shaken at room temperature for an optimized period of time (t = 10 min for ARS, and t = 5 min for BTB). The adsorption capacity of BFA−APTES was found to increase as the pH of the solutions was increased from 2, and the maximum adsorption against both the dyes was obtained at pH 4 (percentage removal: 91% for ARS and 96% for BTB). However, a further increase in the pH of the medium resulted in a decrease in the adsorption capacity. For instance, the adsorption of BTB on BFA−APTES showed an abrupt reduction in adsorption with increasing pH, from 96% (pH 4) to 5% removal (pH 8) (Figure 5b). The high adsorption capacity of BFA−APTES at acidic pH can be attributed to the higher magnitude of positive charge on its surface because of the protonation of surface amino groups. Hence, the positive charge on the surface of BFA−APTES at acidic pH facilitated in enhancing its electrostatic interaction with the polar groups of the anionic dyes ARS (pK_a = 5.49 and 10.85) and BTB (pK_a = 7.3). A slightly lower percentage removal observed at pH 2 compared to pH 4 can be attributed to a higher extent of protonation of sulfonic acid groups resulting in the reduction in net negative change on the dye molecules that led to a reduced electrostatic interaction between BFA−APTES and the dye molecules. Decrease in the adsorption capacities at pH 6 and above can be related to the decrease in the extent of protonation of amino groups, leading to the decrease in the magnitude of surface positive change on BFA−APTES and increase in the extent of the deprotonation of sulfonic acid groups that leads to an increased negative charge on the dye molecules. The deprotonation of functionalities at higher pH results in an increase in the electrostatic repulsion between the exposed lone pair of electrons of amino groups on BFA−APTES surface and negative charge on the dye molecules, which manifests in the form of decrease in the adsorption capacity of BFA−APTES. Performing the adsorption studies at pH 4 would protonate all the functional groups of the anionic dyes. This suggests that the adsorption process seems to be primarily driven by the extent interaction between the protonated surface amino groups of BFA−APTES and polar groups present in the dye molecules.

The adsorption behavior of A-BFA against both dyes was completely different. A-BFA is microporous and contain many −OH groups on the surface. It is well known that the free vibrating −OH groups are strong adsorption sites, particularly with lone pair adsorbates (such as SO_3, O═ and Br groups).[56] Each −OH group acts as a specific adsorption site for aromatic groups of dye molecules resulting in some degree of adsorption (40−45%) at pH between 2 and 6 for both dyes. However,

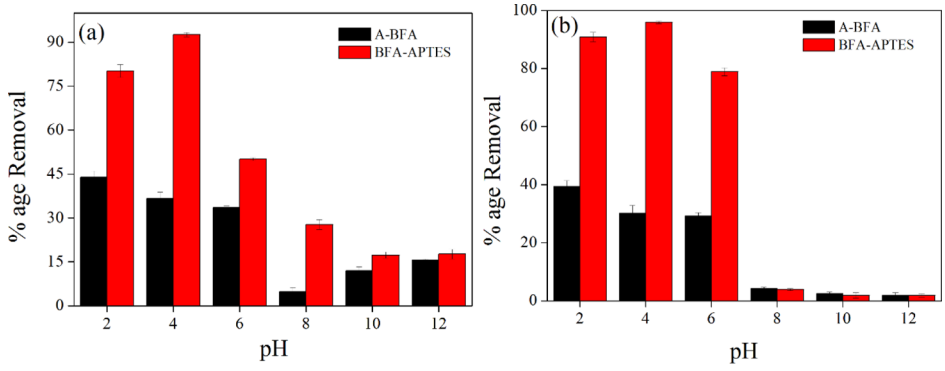

Figure 5. Effect of pH on the %age removal of (a) ARS (t = 10 min, amount of adsorbents = 20 mg, at room temperature); (b) BTB (t = 5 min, amount of adsorbents = 20 mg, at room temperature).

https://dx.doi.org/10.1021/acsomega.0c00889
ACS Omega 2020, 5, 15850−15864

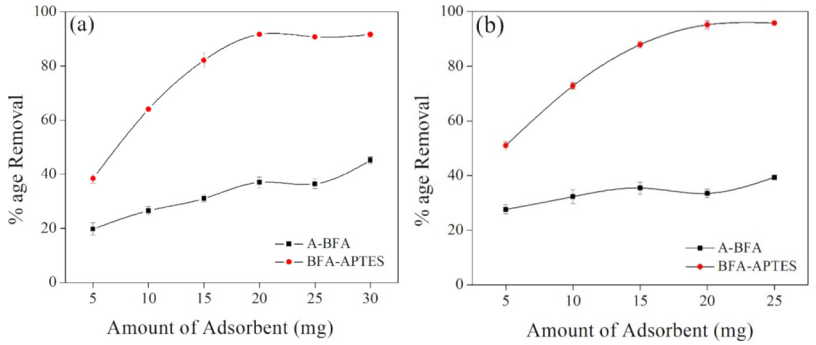

Figure 6. Effect of the amount of adsorbent on the % age removal of (a) ARS (pH = 4, t = 10 min, at room temperature) and (b) BTB (pH = 4, t = 5 min, at room temperature). The solid lines are drawn to highlight the trend.

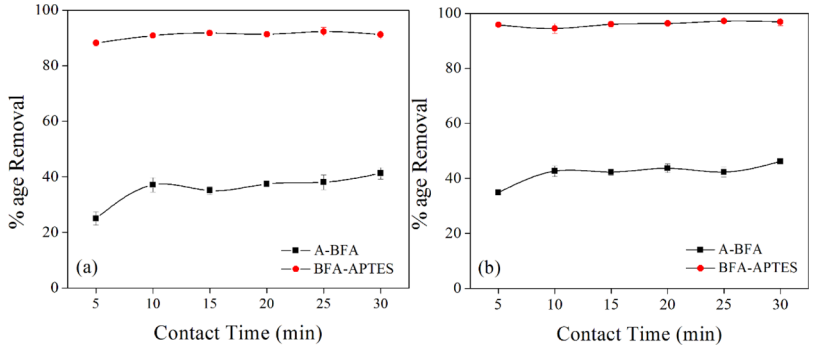

Figure 7. Effect of contact time on the % age removal of (a) ARS (adsorbents = 20 mg, pH = 4 at room temperature); (b) BTB (amount of adsorbents = 20 mg, pH = 4 at room temperature). The solid lines are drawn to highlight the trend.

small adsorption of ARS at higher pH (>7) may be because of nonspecific adsorption into mesopores. There is also the capillary effect. Because BTB is a relatively large molecule, it might not reach the mesopores; hence, a very limited adsorption was observed at higher pH values. A comparison of the adsorption capacities of BFA−APTES and A-BFA clearly highlights superior adsorption capacity for BFA−APTES (Figure 5), which stems from the lack of any amino groups on the surface of nonfunctionalized BFA.

2.2. Effect of Amount of Adsorbent. The effect of amount of adsorbent on the removal capacity of dye was investigated by varying the amounts of A-BFA and BFA−APTES adsorbents (5, 10, 15, 20, 25, and 30 mg). For this purpose, specific amounts of adsorbents were added in 10 mL dye solutions (15 ppm for ARS and 10 ppm for BTB) at room temperature with optimized pH and contact time (pH = 4, t = 10 min for and pH = 4, t = 5 min for BTB). For both dyes, BFA−APTES exhibited higher adsorption capacity as compared to the A-BFA (Figure 6). For 20 mg of adsorbent, the %age removal of ARS dye was found to be 91%, when BFA−APTES was used as the absorbent, which is ∼2.5 times higher than the % age removal of 37%, when nonfunctionalized BFA was used as the adsorbent. Similarly, employing 20 mg of adsorbent, the BFA−APTES adsorbent showed ∼2.9 times higher %age removal toward BTB dye (96% removal) when compared to the nonfunctionalized BFA (33% removal) employed as an adsorbent. Compared to the nonfunctionalized BFA, the superior adsorption capacity of BFA−APTES can be attributed to the presence of amino groups present on the surface of BFA−APTES. Although a slight increase in the percentage adsorptions was observed at adsorbent amounts higher than 20 mg, the subsequent adsorption studies were carried out using 20 mg of adsorbents for the sake of simplicity and process efficiency.

2.3. Effect of Contact Time. In order to determine the optimum time required for the maximum uptake of dye by the BFA−APTES adsorbent, the effect of contact time on the adsorption of dyes was studied for different time intervals ranging from 5 to 30 min (Figure 7). Twenty milligrams of A-BFA and BFA−APTES adsorbents were added to 10 mL of aqueous solutions of dyes (15 ppm for ARS and 10 ppm for BTB), and the suspension was shaken at room temperature for a set interval of time. With the increase in contact time, an increase in the uptake of dyes was observed for both adsorbents. Percentage adsorption of ARS was observed to be around 91% for BFA−APTES and 37% for BFA after a contact time of 10 min, whereas the percentage adsorption of BTB reached 96% for BFA−APTES and 33% for A-BFA after 5 min of exposure to the respective adsorbents. A further increase in the contact time did not result in any appreciable increase in the removal percentage, and for the sake of process simplicity and efficiency, all the subsequent adsorption studies were performed using contact times of 10 min for ARS and 5 min for BTB.

2.4. Effect of Initial Concentration of Dyes. A given amount of adsorbent has the capacity to adsorb only a certain amount of adsorbate species. Thus, the initial concentration of the adsorbate solution plays an important in the adsorption process. To investigate the effect of initial concentration of dyes on the removal capability of adsorbents, the adsorption experiments were carried out at different initial concentrations of dyes (ARS and BTB). Twenty milligrams of A-BFA and BFA−APTES adsorbents were added to 10 mL of dyes solutions (10, 20, 30, 40, and 50 mg L^{-1}), and the suspensions

https://dx.doi.org/10.1021/acsomega.0c00889
ACS Omega 2020, 5, 15850−15864

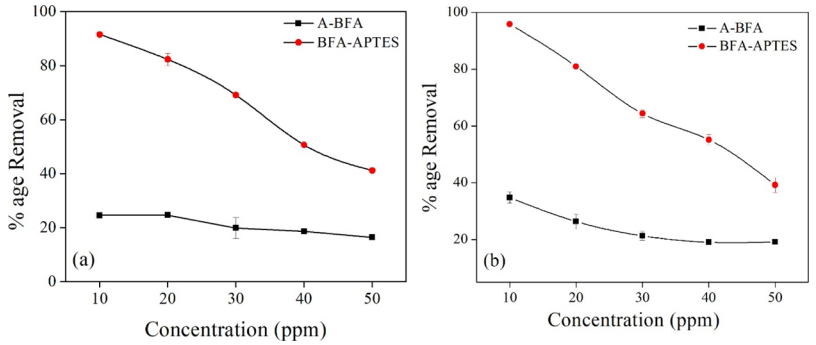

Figure 8. Effect of initial concentration of (a) ARS (adsorbents = 20 mg, pH = 4, contact time = 10 min, at room temperature); (b) BTB (amount of adsorbents = 20 mg, pH = 4, contact time = 5 min, at room temperature) on the % removal by A-BFA and BFA−APTES adsorbents. The solid lines are drawn to highlight the trend.

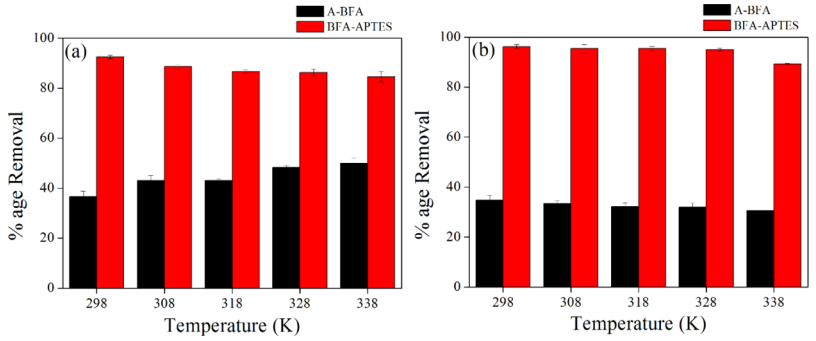

Figure 9. Effect of temperature on the parentage removal of (a) ARS (amount of adsorbents = 20 mg, pH = 4, contact time = 10 min); (b) BTB (amount of adsorbents = 20 mg, pH = 4, contact time = 5 min). The solid lines are drawn to highlight the trend.

were shaken at room temperature for an optimized period of time (t = 10 min for ARS, and t = 5 min for BTB). As apparent from Figure 8, the % age removal of ARS and BTB by both the adsorbents decreased with increasing the initial concentration of dyes. This trend can be attributed to the saturation of the active sites for adsorption on the adsorbent surface at higher concentrations of dyes.

2.5. Effect of Temperature. Influence of temperature on the adsorption properties of A-BFA and BFA−APTES as absorbents was investigated at different temperatures (298, 308, 318, 328, and 338 K). Both the adsorbents (20 mg adsorbent, pH = 4, t = 10 min for ARS, and 20 mg adsorbent, pH = 4, t = 5 min for BTB) were added to 10 mL of aqueous dye solutions (15 ppm for ARS and 10 ppm for BTB). As it is evident from Figure 9, an increase in temperature within the temperature range studied did not have a significant impact on the adsorption capacities of BTB on both A-BFA and BFA−APTES and ARS on BFA−APTES. Weakening of electrostatic interactions between dye molecules and active adsorbent sites at higher temperature could be the main contributor toward the slight decrease in adsorption capacity observed at higher temperatures.[57] A slight increase observed in the case of adsorption of ARS on A-BFA can be because of a better dispersion of the adsorbent and the availability of more binding sites at higher temperature.[58] The change in the adsorption of ARS on BFA−APTES remains within the experimental error limits.

2.6. Adsorption Isotherms. Figure 10 shows both experimental data and nonlinear curve fits for two-parameter and three-parameter models. A comparison of the three isotherms based on SSE values (Table 1) showed that the adsorption of ARS and BTB on BFA−APTES and A-BFA is

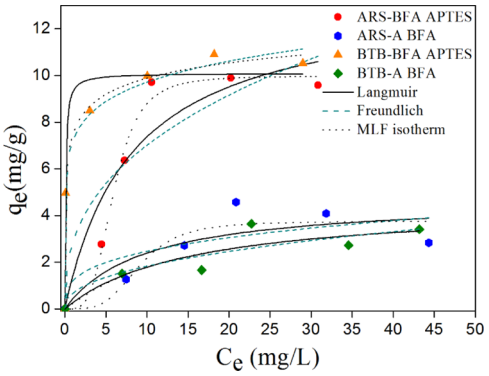

Figure 10. Adsorption isotherms and nonlinear curve fits of Langmuir (black solid line), Freundlich (blue dash line), and MLF (black dots) for ARS-BFA APTES (red circle solid), ARS-A BFA (dark blue hexagon solid), BTB−BFA APTES (orange triangle up solid), and BTB−ABFA (green tilted square solid), respectively.

better estimated by the modified Langmuir−Freundlich (MLF) isotherm. However, R^2 values of the linearized Langmuir isotherm are 0.981 and 0.998, while SSE values are 4.792 and 2.548 for ARS and BTB adsorption on BFA−APTES, respectively. Consequently, comparison between Tables 1 and 2 clearly shows that the use of the R^2 value can be misleading in determining the correct isotherm. Besides, adsorption data of large dye molecules cannot fit to Langmuir because impediments exist between pores and adsorbate; therefore, the value of n is usually less than 1.[59] The maximum adsorption capacities of BFA−APTES for ARS and BTB dye molecules were calculated as 13.42 and 15.44 mg/g, respectively. Meanwhile, the maximum adsorption capacities

https://dx.doi.org/10.1021/acsomega.0c00889
ACS Omega 2020, 5, 15850−15864

Table 1. Adsorption Parameters Obtained from Nonlinear Langmuir, Freundlich, and MLF Isotherm Models at Room Temperature for the Adsorption of ARS and BTB on A-BFA and BFA−APTES

alizarin red S				bromothymol blue			
	parameters	A-BFA	BFA−APTES		parameters	A-BFA	BFA−APTES
Langmuir	q_{max} (mg/g)	4.739	13.417	Langmuir	q_{max} (mg/g)	4.509	10.097
	R_L	0.495	0.439		R_L	0.603	0.008
	SSE	2.047	4.792		SSE	1.532	2.549
Freundlich	K_f (mg/g)	1.211	2.888	Freundlich	K_f (mg/g)	0.681	7.226
	$1/n$	0.309	0.385		$1/n$	0.429	0.128
	SSE	2.511	7.001		SSE	1.611	0.267
MLF	K_{MLF} (L/g)	0.008	0.0011	MLF	K_{MLF} (L/g)	0.060	0.946
	q_{mon} (mg/g)	3.753	9.793		q_{mon} (mg/g)	4.300	15.442
	$1/n$	0.262	0.261		$1/n$	0.931	0.274
	SSE	1.326	0.766		SSE	1.525	0.252

Table 2. Adsorption Parameters Obtained from Linearized Langmuir, Freundlich, and MLF Isotherm Models at Room Temperature for the Adsorption of ARS and BTB on A-BFA and BFA−APTES

alizarin red S				bromothymol blue			
	parameters	BFA	BFA−APTES		parameters	BFA	BFA−APTES
Langmuir	q_{max} (mg/g)	3.762	13.791	Langmuir	q_{max} (mg/g)	4.590	10.761
	R_L	0.364	0.511		R_L	0.640	0.042
	R^2	0.720	0.981		R^2	0.712	0.998
Freundlich	K_f (mg/g)	0.601	1.663	Freundlich	K_f (mg/g)	0.595	6.761
	$1/n$	0.518	0.582		$1/n$	0.467	0.117
	R^2	0.863	0.782		R^2	0.563	0.954
MLF	K_{MLF} (L/mg)	0.191	0.790	MLF	K_{MLF} (L/g)	1.378	28.506
	q_{mon} (mg/g)	407.498	4911.640		q_{mon} (mg/g)	0.737	10.462
	n	4.633	2.678		n	0.584	0.992
	R^2	0.963	0.839		R^2	0.442	0.997

Table 3. Comparison of Adsorption Characteristics of Adsorbents Derived from Various Fly Ash-Based Adsorbents

sr. no	adsorbents	dyes	adsorption capacity q_{max} (mg/g)	time	references
1	coal fly ash	reactive red 23, reactive blue 171, acid black 1, and acid blue 193	2.102, 1.860, 10.331, and 10.937	60 min	60
2	coal fly ash	methylene blue	15.04	120 min	61
3	magnetic chitosan-fly ash (CS-FA/Fe_3O_4)	reactive orange 16 (RO16)	66.9	55 min	62
4	coal fly ash (CFA)	methylene blue	6.409	60 min	63
5	fly ash (FA) modified by $Ca(OH)_2/Na_2FeO_4$	methyl orange	14.76	40 min	64
6	fly ash/$NiFe_2O_4$ composite	congo red	23.33	180 min	65
7	fly ash geopolymer monoliths	methylene blue	15.4	30 h	66
8	magnesium oxide (MgO)/fly ash composite (FAMgO)	RB5 azo dye	48.78	90 min	67
9	BFA−APTES	bromothymol blue	15.44	5 min	current Study
10	BFA−APTES	alizarin red S	13.42	10 min	current Study

of A-BFA were 2−3 times less than BFA−APTES for both dyes (Table 1).

For the sake of comparison, adsorption characteristics of the adsorbents reported in this study were compared with the related adsorbents reported in the literature. Table 3 gives a simple comparison of the adsorption ability of fly ash-derived adsorbent materials for the adsorption of dyes. It is evident from Table 3 that the adsorbents reported in this study exhibited higher adsorption efficiency compared to similar adsorbents, while the adsorption capacities of the absorbents reported in this study were comparable to some of the adsorbents reported in the literature.

The adsorption density (Γ, mg/m^2) or the amount of dyes adsorbed on the active surface of adsorbents at a particular concentration was calculated by using following equation[68]

$$\Gamma = \frac{V\Delta C}{mS} \quad (1)$$

where V is the volume of liquid phase (L), ΔC is the difference between the initial and final concentrations of adsorbates in aqueous solution, m is the mass of adsorbent (g), and S is the surface area (m^2/g). Using this relation, the adsorption density or the amount of dyes adsorbed on the active surface of adsorbents at a particular residual concentration can be calculated. The adsorption density of ARS and BTB per unit

https://dx.doi.org/10.1021/acsomega.0c00889
ACS Omega 2020, 5, 15850−15864

Table 4. Comparison of Adsorption Densities of Various Adsorbents Reported in the Literature

sr. no.	adsorbents	adsorbates	adsorption density Γ	references
1	mesoporous alumina	As(III), As(V)	1.94×10^{-6}, 5.85×10^{-6} mol/m^2	68
2	mesoporous Alumina	ammonia	0.44 mg/m^2	69
3	γ-Al_2O_3/Fe_3O_4/SiO_2/PGMA nanocomposite	remazol navy RGB azo dye	1.30 mg/m^2	70
4	sepiolite	Co(II)	$1:17 \times 10^{-6}$ mol/m^2	71
5	BFA−APTES	bromothymol blue	0.608 mg/m^2	current study
6	BFA−APTES	alizarin red S	0.306 mg/m^2	current study

surface area of APTES−BFA was found to be 0.306 and 0.608 mg/m^2. Interestingly, these grafting densities translate into 5.11×10^{17} and 6.56×10^{17} molecules of ARS and BTB per m^2 of the adsorbent (BFA−APTES). The number of dye molecules per unit area are slightly less than the number of APTES molecules that were estimated to be grafted on the surface (7.35×10^{18} molecules) which can be because of the steric bulk of the dye molecules that need more surface area while adsorbing on the surface. With this data, we can conclude that the surface of the adsorbent is reasonably saturated.

Table 4 gives a comparison of the amount of adsorbent adsorbed per unit surface area of different adsorbent materials reported in the literature and the adsorbent reported in this study.

2.7. Adsorption Kinetics. Adsorption rate constants were calculated by measuring instantaneous adsorption capacity (q_t) as a function of time. A comparison of linear and nonlinear forms of pseudo-first- and pseudo-second-order kinetics models is graphically demonstrated in Figure 11 for ARS

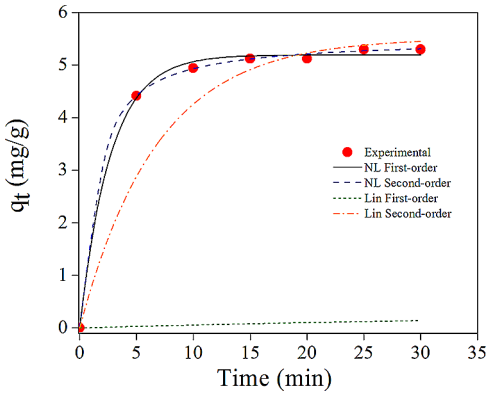

Figure 11. Comparison of adsorption kinetics estimated by the nonlinear curve fits (black solid line for pseudo-first-order and dashed blue line for pseudo-second-order kinetics) and linear curve fits (green dotted line for pseudo-first-order and orange dashdotted line for pseudo-second-order kinetics) for the adsorption of ARS−BFA APTES (red circle solid).

adsorption on BFA−APTES, while the kinetic rate constants, SSE, and correlation coefficient (R^2) of both models for all the samples are summarized in Tables 5 and 6. It is clear that the nonlinear analysis produced the best curve fits, providing estimations that were the closest to the experimental data. A reasonable agreement between the calculated and experimental values of q_e obtained from the nonlinear form of kinetic models verifies the importance of using equations in their original form.[59] Adsorption of both dyes on BFA−APTES has the fastest rates (k_2 = 1.395 g/mg min for BTB and k_2 = 0.518 g/mg min for ARS).

The difference between the constants (k_1, k_2, and q_e) obtained from linear and nonlinear kinetic models appear to be very clear between Tables 5 and 6.

After this step, kinetic constants with the lowest SSE value will be used in our calculations. We assume that adsorption kinetics follows the Arrhenius type behavior.

$$k = A \exp^{(-E_a/RT)} \tag{2}$$

and

$$\Delta_{ad}H^0_m = E_a - RT \tag{3}$$

The adsorption molar enthalpy ($\Delta_{ad}H^0_m$) is calculated for both dyes on A-BFA and BFA−APTES from the nonlinear curve fitted plots of reaction rate constant (k) versus temperature (Table 7).

2.8. Adsorption Thermodynamics. The thermodynamic parameters such as adsorption molar Gibbs free energy ($\Delta_{ad}G^0_m$), adsorption molar enthalpy ($\Delta_{ad}H^0_m$), and adsorption molar entropy ($\Delta_{ad}S^0_m$) were studied to investigate the effect of temperature on the adsorption process at pH 4.[72,73] The magnitude of $\Delta_{ad}G^0_m$ was calculated from following equation

$$\Delta_{ad}G^0_m = -RT \ln K \tag{4}$$

where K is the equilibrium constant ($K = k_{ads}/k_{des}$), T is the absolute temperature (K), and R is the universal gas constant (8.314 J/mol K).

The adsorption molar enthalpy $\Delta_{ad}H^0_m$ and $\Delta_{ad}S^0_m$ were obtained from Van't Hoff relation

$$\ln K = \frac{\Delta_{ad}S^0_m}{R} - \frac{\Delta_{ad}H^0_m}{RT} \tag{5}$$

The calculated thermodynamic parameters are summarized in Table 7. A study of temperature dependence of the adsorption process gives information on the spontaneity of the adsorbent−adsorbate interaction.[74] The ΔG^0 values in the range of 0 to −20 and −80 to −400 kJ mol^{-1} indicate physical and chemical adsorption processes, respectively.[75] The negative values of $\Delta_{ad}G^0_m$ observed in our study suggested a spontaneous nature of the process of adsorption of dyes on BFA−APTES, whereas a positive $\Delta_{ad}G^0_m$ was calculated for A-BFA, which indicated unfavorable adsorption on this adsorbent. The negative values of $\Delta_{ad}H^0_m$ indicated the exothermic nature of adsorption processes.

It is worth mentioning here that the temperature range of 298−338 K was applied in this study to demonstrate the adsorption behavior of the reported adsorbent under the conditions that can be conveniently applied at large scales. In addition, the 298−338 K temperature range is widely employed by other researchers, which would make it convenient to draw comparisons between different studies.[76−79]

https://dx.doi.org/10.1021/acsomega.0c00889
ACS Omega 2020, 5, 15850−15864

Table 5. Nonlinear Pseudo-First-Order and Pseudo-Second-Order Kinetics Analysis Results for the Adsorption of ARS and BTB on A-BFA and BFA−APTES

alizarin red S				bromothymol blue			
	parameters	A-BFA	BFA−APTES		parameters	A-BFA	BFA−APTES
pseudo-first-order	q_e(mg/g) experimental	1.339	5.296	pseudo-first-order	q_e(mg/g) experimental	4.316	10.140
	q_e (mg/g) calculated	1.964	5.194		q_e (mg/g) calculated	3.998	10.033
	k_1 (min^{-1})	0.325	0.369		k_1 (min^{-1})	0.604	1.246
	SSE	0.271	0.033		SSE	0.032	0.042
pseudo-second-order	q_e (mg/g) experimental	1.339	5.296	pseudo-second-order	q_e (mg/g) experimental	4.316	10.140
	q_e (mg/g) calculated	2.023	5.516		q_e (mg/g) calculated	4.107	10.088
	k_2 (g/mg min)	0.518	0.148		k_2 (g/mg min)	0.544	1.395
	SSE	0.339	2.896		SSE	0.076	0.049

Table 6. Linearized Pseudo-First-Order and Pseudo-Second-Order Kinetics Analysis Results for the Adsorption of ARS and BTB on A-BFA and BFA−APTES

alizarin red S				bromothymol blue			
	parameters	A-BFA	BFA−APTES		parameters	A-BFA	BFA−APTES
pseudo-first-order	q_e (mg/g) experimental	1.339	5.296	pseudo-first-order	q_e (mg/g) experimental	4.316	10.140
	q_e (mg/g) calculated	0.491	0.312		q_e (mg/g) calculated	0.644	0.033
	k_1 (min^{-1})	0.020	0.020		k_1 (min^{-1})	0.020	0.152
	R^2	0.05	0.27		R^2	0.19	0.34
pseudo-second-order	q_e (mg/g) experimental	1.339	5.296	pseudo-second-order	q_e (mg/g) experimental	4.316	10.140
	q_e (mg/g) calculated	1.114	5.520		q_e (mg/g) calculated	4.440	10.181
	k_2 (g/mg min)	0.122	0.153		k_2 (g/mg min)	0.223	0.474
	R^2	0.94	0.99		R^2	0.98	0.99

Table 7. Thermodynamic Parameters for the Adsorption of ARS and BTB on BFA and BFA-APTES.

alizarin red S			bromothymol blue		
parameters	A-BFA	BFA−APTES	parameters	A-BFA	BFA−APTES
$\Delta G°$ (kJ/mol)	5.839	−1.300	$\Delta G°$ (kJ/mol)	3.787	−11.647
$\Delta H°$ (kJ/mol)	−21.948	−13.393	$\Delta H°$ (kJ/mol)	−10.585	−87.817
$\Delta S°$ (kJ/mol.K)	−0.093	−0.042	$\Delta S°$ (kJ/mol.K)	−0.048	−0.256

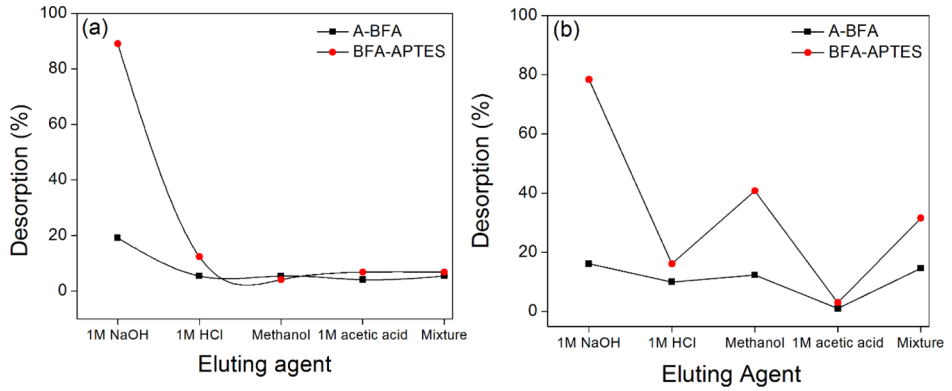

Figure 12. Effect of different eluting agents on desorption of dyes (a) ARS (amount of adsorbent = 20 mg, t = 10 min, at room temperature) and (b) BTB (amount of adsorbents = 20 mg, t = 5 min, at room temperature). The solid lines are drawn to highlight the trend.

2.9. Regeneration and Reusability. Regeneration of the adsorbent after the adsorption process is important for its reuse especially for increasing the economic feasibility of the process at commercial scale. Different eluting agents including NaOH, HCl, methanol, acetic acid, and a mixture of methanol and acetic acid were employed to regenerate the adsorbent for reuse.[80] The desorption of dyes was carried out by separately washing the ARS (t = 10 min, T = 298 K) and BTB (t = 5 min, T = 298 K) loaded adsorbents with different eluting agents, 10 mL of 1 M NaOH, 1 M HCl, methanol, 1 M acetic acid, and a mixture of acetic acid and methanol (1:1). The concentrations of desorbed dye in solutions were spectrophotometrically quantified. The best desorption performance was achieved with 1 M NaOH solution for ARS (89%) and BTB (79%) (Figure 12). The superior desorption performance of NaOH highlights that the interaction between the BFA−APTES adsorbent and dyes (ARS and BTB) is electrostatic in nature with high dependency on the pH of the medium. This observation complements our results provided in the previous

https://dx.doi.org/10.1021/acsomega.0c00889
ACS Omega 2020, 5, 15850−15864

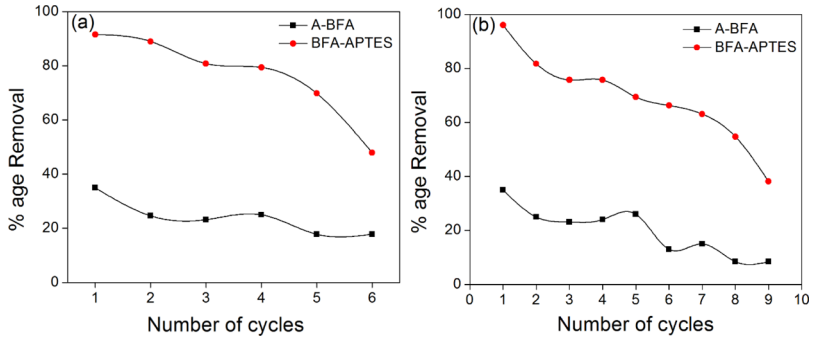

Figure 13. Reusability of A-BFA and BFA−APTES for the adsorption of (a) ARS (amount of adsorbent = 20 mg, pH = 4, t = 10 min, at room temperature) and (b) BTB (amount of adsorbent = 20 mg, pH = 4, t = 5 min, at room temperature). The solid lines are guide to the eye.

section of this study dealing with the effect of pH on adsorption capacity of the reported adsorbent.

After successful demonstration of regeneration of adsorbents, their reusability was also studied. For the regeneration of adsorbents, the dye-loaded A-BFA and BFA−APTES were separately dispersed in 10 mL of 1 M NaOH solution under optimized conditions (for ARS t = 10 min, at room temperature and for BTB t = 5 min, at room temperature). After desorption, adsorbents were washed with deionized water, dried at 80 °C, and reused for adsorption in the next cycle. Meanwhile, the concentrations of the released dyes in the supernatants were determined spectrophotometrically. To validate the reusability of A-BFA and BFA−APTES, several cycles of consecutive adsorption−desorption were carried out. The results displayed in Figure 13 showed that the BFA−APTES showed more than 60% removal for up to 5 cycles for ARS and for up to 6 cycles for BTB.

As it can be noticed from this study, BFA by its nature is a poor adsorbent; however, it can be modified to achieve a better performance.[81] Silanization is a low-cost and effective covalent coating method to modify material surfaces. A number of silane-coupling agents are commercially available, which can conveniently introduce a variety of functional groups (e.g., amino group and carboxyl group) on diverse surfaces presenting hydroxyl groups.[82] APTES, the silane employed in this study, is the most widely used silane employed for the surface functionalization to achieve materials displaying amino groups on their surfaces.[83] Thus, in the present work, the development of the adsorbent involves inexpensive raw materials (BFA and APTES) and simple functionalization process. The abundance of these materials, low cost, modest processing, and reasonable adsorption ability make our reported adsorbent (APTES−BFA) an attractive platform from sustainability as well as the economic point of view. It is worth mentioning here that considering the low cost related to the materials and the process applied in this study, reusability might be of limited importance; however, we believe that the reusability experiment presented here is of high scientific interest for the scientific community which is working on the development of cost-effective adsorbents for remediation applications.

2.10. Column Studies. BFA−APTES was chosen as the model adsorbent in batch experiments because of its aforementioned superior adsorption characteristics. A small column of the BFA−APTES adsorbent is packed to demonstrate its remediation properties in column setting. A simple glass tube (pasture pipette) with a diameter of 6 mm and a length of 22 mm is used for this purpose. A small plug of glass wool was placed at the bottom of the column (Figure 14) to prevent washing out of the adsorbent. Each adsorbent (500 mg) (A-BFA and BFA−APTES) was added to two separate columns followed by the gentle tapping of the columns to consolidate the adsorbents and remove any air bubble. ARS dye solution was chosen as an adsorbate because of its ease of visual following with 200 ppm concentration (Figure 14). It was observed that the column packed with the BFA−APTES adsorbent could remove 99% of dye (ARS) from the 15 mL of 200 ppm dye solution passed through it. The water coming out of the column packed with the BFA−APTES adsorbent was clear without any visible trace of dye in it that was also confirmed spectrophotometrically (please refer to the video provided in Supporting Information). On the other hand, red-colored water can be clearly seen coming out of the column packed with A-BFA. It is worth mentioning here that the aqueous solution of ARS dye is yellowish in color under acidic and neutral conditions. Because of the pH responsiveness, ARS shows red color under basic conditions. The basic nature of A-BFA led to the change in color of ARS dye to red while it passed through the column packed with the A-BFA.

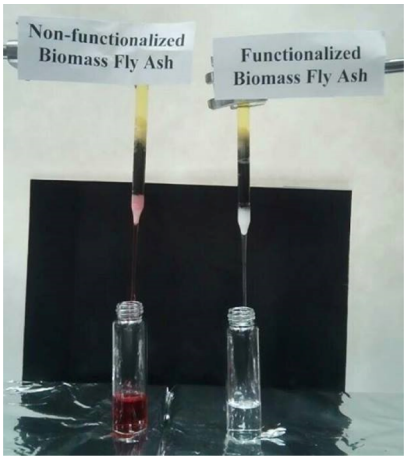

Figure 14. Photograph of columns packed with the A-BFA and BFA−APTES adsorbents. 200 ppm aqueous solution of ARS dye was passed through both the columns. The water coming out of the columns was collected in glass vial for spectrophotometric estimation of the dye content.

3. CONCLUSIONS

In summary, we presented silanization as a facile route for the functionalization of pristine BFA to prepare efficient

https://dx.doi.org/10.1021/acsomega.0c00889
ACS Omega 2020, 5, 15850−15864

adsorbents for the adsorptive removal of anionic dyes (ARS and BTB). We simply employed APTES to prepare amine-functionalized BFA (BFA−APTES). The effectiveness of the employed strategy for the fabrication of BFA−APTES and the physiochemical properties of the resulting material were established by employing XPS, SEM, and TGA. The prepared BFA−APTES was applied as an adsorbent for the adsorptive removal of anionic dyes (ARS and BTB). The adsorption behavior of A-BFA and BFA−APTES was quantified and compared with linear and nonlinear versions of isotherm and kinetic models. Our comparative calculations have shown that linearizing adsorption equations can be misleading and incomplete. The nonlinear analysis on experimental data is the most accurate calculation method, and it is simple. The BFA−APTES absorbent displayed superior adsorption capacities toward both the dyes tested in this study. The superior adsorption capacities in the case of BFA−APTES were attributed to the successful introduction of amine groups on the surface of BFA during the silanization process. The adsorption behavior was found to follow the MLF adsorption model. The thermodynamic parameters including $\Delta_{ad}G_m^0$ and $\Delta_{ad}H_m^0$ suggested that the process of adsorption was spontaneous and exothermic. The developed BFA−APTES adsorbent also exhibited superior recyclability and could be reused for several cycles after desorption of the adsorbed dyes. Besides studying the remediation in batch setting, we also packed columns using A-BFA and amine-functionalized BFA. Our column studies further revealed the superior performance of BFA−APTES for efficient removal of dye from aqueous solution. Based on the data presented in this study, we believe that this simple and low-cost modification approach opens up new opportunities for the fabrication of BFA-based functional materials as efficient adsorbents for remediation applications.

4. EXPERIMENTAL SECTION

4.1. Materials and Methods. BFA was obtained from a biomass thermal power station installed at Bulleh Shah Packaging (Ltd.), Kasur, Pakistan. Wheat and corn stalks constitute the major part of the biomass fuel. Toluene (99%), APTES (≥98%), BTB (95%), ethanol (>99%), acetic acid (99.7%), and methanol (>99%) were purchased from Sigma-Aldrich, Germany. ARS was purchased from Eyer Chemical reagents, China.

4.2. Activation of BFA. BFA was washed several times with distilled water to remove any water-soluble contents. After washing, BFA was dried in an oven at 100 °C for 24 h. The activation of BFA was achieved by stirring its suspension in 1 M aqueous HCl solution for 24 h. The activated fly ash was recovered by gravity filtration and washed several times with water to remove any residue HCl. The activated BFA (A-BFA) was then dried in an oven at 100 °C for 24 h. The acid treatment of fly ash improves the adsorption characteristics by removing soluble impurities present in FA and exposing the surface −OH groups.

4.3. Synthesis of Amine-Functionalized BFA (BFA−APTES). APTES functionalization of BFA (BFA−APTES) was performed using a slightly modified version of the reported procedures.[42,43,84−86] APTES (4 mL) was added in 36 mL of toluene; 2 g of activated BFA was added in this solution, and the suspension was refluxed for 24 h. The product was then centrifuged, washed three times with toluene, and dried in an oven at 100 °C overnight.

4.4. Structural Characterization. SEM was performed using FEI Nova Nano SEM 450 equipped with the Oxford EDX detector. XPS was performed using Thermo Scientific K-Alpha. The Mg Kα (1253.6 eV) X-ray source was operated at 300 W. A pass energy of 117.40 eV was used for the survey scans. The spectra were recorded using a 60° take off angle relative to the surface normal. TGA was carried out on a TGA Q50 V6.2 Build 187 thermogravimetric analyzer. Samples were heated at 10 °C min^{-1} from ambient temperature to 800 °C under nitrogen flow. The UV/vis absorption spectra were recorded using a Shimadzu UV-1800 spectrophotometer. The N_2 adsorption−desorption measurements were performed by using a Quantachrome Nova 2200e. Prior to the measurements, A-BFA and BFA−APTES were degassed overnight under vacuum at 363 and 333 K, respectively.

4.5. Batch Adsorption Studies. The dye adsorption capacities of A-BFA and BFA−APTES were studied by a batch method, which permits a convenient evaluation of parameters that influence the adsorption process, such as chemical modification, pH of dye solutions, initial concentration of dyes, amount of adsorbents, contact time, and temperature. The effect of pH was investigated by preparing a series of dye solutions with pH ranging from 2.0 to 12.0 at a concentration of 15 mg L^{-1}. The pH of the dye solution was adjusted with 0.1 M HCl or 0.1 M NaOH aqueous solutions. The effect of dye concentration was monitored by using different initial concentrations of dye solutions (10, 20, 30, 40, and 50 mg L^{-1}) at the pH optimal for adsorption. The impact of the dosage amount was determined by adding different amounts (5−30 mg) of adsorbents (A-BFA and BFA−APTES) to the dye solutions at the pH optimal for adsorption. To study the effect of contact time, the dye content remained in the solution treated with the adsorbents at predetermined time intervals (5, 10, 15, 20, 25, and 30 min) was determined spectrophotometrically. The effect of temperature on the adsorption of dyes was studied by performing adsorption at different temperatures (298, 308, 318, 328, and 338 K). In each adsorption experiment, 10 mL of dye solutions were used and the suspensions were shaken at 250 rpm. After shaking at the optimized conditions, the samples were centrifuged and the concentrations of dyes in the supernatant solutions were determined using a spectrophotometer. The calibration curves were obtained by recording absorbance of dye solutions of known concentrations at λ_{max} (422 nm for ARS and 432 nm for BTB). Different reagents (1 M NaOH, 1 M HCl, methanol, 1 M acetic acid, and a 1:1 by volume mixture of methanol and acetic acid) were tested for regeneration of the used adsorbents. To study the reusability of both the adsorbents, the dye-loaded A-BFA and BFA−APTES were separately dispersed in 10 mL of 1 M NaOH solution. After desorption, adsorbents were washed with deionized water, dried, and reused for the next adsorption cycle. The concentrations of the desorbed dyes in the supernatants were determined spectrophotometrically.

The column adsorption studies were conducted in a glass column with a diameter of 6 mm and a length of 22 mm. Known quantities (500 mg) of both adsorbents (A-BFA and BFA−APTES) were packed in separate columns to yield the desired bed height of the adsorbent; 200 ppm solution of ARS dye was channeled into the column. Samples of the water coming out of the column were collected and analyzed spectrophotometrically to estimate the concentration of dye.

https://dx.doi.org/10.1021/acsomega.0c00889
ACS Omega 2020, 5, 15850−15864

The amount of dye adsorbed at equilibrium q_e (mg/g) was calculated from the following equation

$$q_e = \frac{(C_o - C_e)V}{W} \quad (6)$$

where, q_e is the adsorption capacity (mg/g) of the adsorbent at equilibrium, V is the volume of dye aqueous solution in litres, C_o and C_e (mg/g) are the initial and equilibrium concentrations of dye, and W is the mass of the adsorbent in grams.

Please note that the dyes can photobleach overtime, and this aspect should be considered by performing the dye removal experiments that are based on UV/vis absorption of the dye solutions. In our case, we monitored the UV/vis absorption of 15 ppm solution of ARS and 10 ppm solution of BTB for three consecutive days (stored in the dark) and observed that upon careful storage, there was no change in the intensity of absorption for both the dyes during first two days. A small decrease in the intensity of absorption of both the dyes was observed on the third day; however, this timeframe is beyond the timeframe used in the remediation experiments reported in this study. Therefore, photobleaching does not contribute to the data presented in this study.

4.6. Adsorption Isotherms. Adsorption of ARS and BTB onto A-BFA and BFA−APTES was investigated by two-parameter (Langmuir and Freundlich) and three-parameter (MLF) nonlinear models. The langmuir model describes that the adsorbent sites have identical energy, and each adsorbate molecule is located on a single site. This model depicts the formation of the monolayer of the adsorbate on the homogeneous adsorbent surface. The nonlinear form of Langmuir isotherm is given as

$$q_e = \frac{K_L q_{max} C_e}{1 + K_L C_e} \quad (7)$$

while the linearized Langmuir isotherm is

$$\frac{C_e}{q_e} = \frac{1}{q_{max} K_L} + \frac{C_e}{q_{max}} \quad (8)$$

where C_e is the equilibrium concentration of the adsorbate (mg L^{-1}), q_e is the amount of the adsorbate adsorbed per unit amount of the adsorbent at equilibrium (mg g^{-1}), and q_{max} (mg g^{-1}) and K_L (L mg^{-1}) are the Langmuir constants related to maximum monolayer adsorption capacity and energy change during adsorption.[84]

The dimensionless separation factor (R_L) is generally used to express the feasibility of adsorption and affinity between the adsorbent and adsorbate. The value of R_L indicates the shape of the isotherm to be either unfavorable ($R_L > 1$), linear ($R_L = 1$), favorable, ($0 < R_L < 1$) or irreversible ($R_L = 0$)[87] and can be calculated by the following equation

$$R_L = \frac{1}{K_L C_0 + 1} \quad (9)$$

where C_o (mg L^{-1}) is the initial concentration of the adsorbate. In the present study, the calculated R_L values were in the range of $0 < R_L < 1$, indicating favorable adsorption of dye molecules on both the adsorbents.

The Freundlich isotherm is not restricted to the formation of the monolayer and describes the nonideal adsorption that involves the heterogeneous surfaces. The nonlinear Freundlich isotherm is expressed as

$$q_e = K_f C_e^{1/n} \quad (10)$$

whereas the linearized Freundlich isotherm equation is

$$\log q_e = \log K_f + \frac{1}{n} \log C_e \quad (11)$$

where q_e represents dye concentration adsorbed on an adsorbent (mg g^{-1}) at equilibrium, K_f is the Freundlich constant which represents the adsorption capacity (mg g^{-1}), C_e represents equilibrium dye concentration in solutions (mg L^{-1}), and the slope, $1/n$ with favorable range between 0 and 1, is a measure of the adsorption intensity or surface heterogeneity.[43] The calculated values of $1/n$ are 0.58 ± 0.12 and 0.11 ± 0.07 for the adsorption of ARS and BTB on BFA−APTES, respectively. The smaller value of $1/n$ for BTB indicated better interaction with the adsorbent and hence more favorable adsorption of BTB on BFA−APTES than ARS.

The MLF is a three-parameter empirical model, and there is linear dependency on the concentration in the numerator and exponentially increases in the denominator to enhance the wide range of concentration of adsorption equilibrium.

$$q_e = \frac{q_{mon} K_{MLF} C_e^{1/n}}{1 + K_{MLF} C_e^{1/n}} \quad (12)$$

and the linearized MLF model can be written as

$$\ln\left(\frac{q_e}{q_{mon} - q_e}\right) = \frac{1}{n}\ln(C_e) + \ln(K_{MLF})^{1/n} \quad (13)$$

where q_{mon} is the adsorption capacity (mg g^{-1}), and K_{MLF} (L mg^{-1}) and n are the MLF constants. The value of $1/n$ lies between zero and unity.

The linear regression coefficient (R^2) and least-square regression based on the sum of the squares of residues (SSE) are applied as error functions in order to identify the best adsorption isotherms and kinetic models for linear and nonlinear forms of corresponding models.

$$SSE = \sum_{i=1}^{m} (q_{e,pre} - q_{e,exp})^2 \quad (14)$$

4.7. Adsorption Kinetics. Kinetics of the adsorption process provides essential information about the reaction pathways and the solute uptake rate. The linear forms of pseudo-first-order and pseudo-second-order kinetics were applied to study the adsorption kinetics.[88] The nonlinear pseudo-first-order model was described as

$$q_t = q_e(1 - \exp^{-k_1 t}) \quad (15)$$

While linear version of the pseudo-first-order model was described by Lagergren

$$\log(q_e - q_t) = \log q_e - \left(\frac{k_1}{2.303}\right)t \quad (16)$$

where q_e and q_t are the adsorption capacities (mg g^{-1}) at equilibrium and at time t, respectively, and k_1 is the rate constant of pseudo-first-order adsorption (L min^{-1}).

The nonlinear pseudo-second-order rate equation is

$$q_t = \frac{q_e^2 k_2 t}{1 + q_e k_2 t} \quad (17)$$

https://dx.doi.org/10.1021/acsomega.0c00889
ACS Omega 2020, 5, 15850−15864

and linear from of pseudo-second-order rate equation of McKay and Ho can be expressed as

$$\frac{t}{q_t} = \frac{1}{k_2 q_e^{\ 2}} + \frac{1}{q_e} t \tag{18}$$

where the equilibrium adsorption capacity q_e and the pseudo-second-order constants k_2 (g/mg min) can be determined experimentally.

■ ASSOCIATED CONTENT

Supporting Information

The Supporting Information is available free of charge at https://pubs.acs.org/doi/10.1021/acsomega.0c00889.

Demonstration of remediation on the column packed with the developed adsorbent (MP4)

■ AUTHOR INFORMATION

Corresponding Authors

Hatice Duran − *Department of Materials Science & Nanotechnology Engineering, TOBB University of Economics and Technology, 06560 Ankara, Turkey;* orcid.org/0000-0001-6203-3906; Email: hduran@etu.edu.tr

Basit Yameen − *Department of Chemistry & Chemical Engineering, Syed Babar Ali School of Science and Engineering (SBASSE), Lahore University of Management Sciences (LUMS), Lahore 54792, Pakistan;* orcid.org/0000-0002-4359-8394; Email: basit.yameen@lums.edu.pk

Authors

Safana Dogar − *Department of Chemistry & Chemical Engineering, Syed Babar Ali School of Science and Engineering (SBASSE), Lahore University of Management Sciences (LUMS), Lahore 54792, Pakistan*

Sana Nayab − *Department of Chemistry & Chemical Engineering, Syed Babar Ali School of Science and Engineering (SBASSE), Lahore University of Management Sciences (LUMS), Lahore 54792, Pakistan*

Muhammad Qamar Farooq − *Department of Chemistry & Chemical Engineering, Syed Babar Ali School of Science and Engineering (SBASSE), Lahore University of Management Sciences (LUMS), Lahore 54792, Pakistan*

Amir Said − *Bulleh Shah Packaging (BSP) Pvt. Ltd., Kasur, Pakistan*

Raheel Kamran − *Bulleh Shah Packaging (BSP) Pvt. Ltd., Kasur, Pakistan*

Complete contact information is available at: https://pubs.acs.org/10.1021/acsomega.0c00889

Author Contributions

The manuscript was written through contributions of all authors. All authors have given approval to the final version of the manuscript.

Notes

The authors declare no competing financial interest.

■ ACKNOWLEDGMENTS

B.Y. acknowledges support from HFSP (RGY0074/2016), HEC for NRPU (Project no. 20-1740/R&D/10/3368, 20-1799/R&D/10-5302, and 5922), TDF-033 grants, and LUMS for start-up fund and FIF grant. H.D. gratefully acknowledges Max−Planck−Gesellschaft (MPG) for the financial support of the MPIP-TOBB ETU Partner Group Program (Soft Matter in Nanoconfinement).

■ REFERENCES

(1) McKendry, P. Energy production from biomass (part 1): overview of biomass. *Bioresour. Technol.* **2002**, *83*, 37−46.

(2) Voshell, S.; Mäkelä, M.; Dahl, O. A review of biomass ash properties towards treatment and recycling. *Renew. Sustain. Energy Rev.* **2018**, *96*, 479−486.

(3) Xing, Y.; Guo, F.; Xu, M.; Gui, X.; Li, H.; Li, G.; Xia, Y.; Han, H. Separation of unburned carbon from coal fly ash: A review. *Powder Technol.* **2019**, *353*, 372−384.

(4) Blissett, R. S.; Rowson, N. A. A review of the multi-component utilisation of coal fly ash. *Fuel* **2012**, *97*, 1−23.

(5) Izquierdo, M.; Querol, X. Leaching behaviour of elements from coal combustion fly ash: An overview. *Int. J. Coal Geol.* **2012**, *94*, 54−66.

(6) Yao, Z. T.; Ji, X. S.; Sarker, P. K.; Tang, J. H.; Ge, L. Q.; Xia, M. S.; Xi, Y. Q. A comprehensive review on the applications of coal fly ash. *Earth-Sci. Rev* **2015**, *141*, 105−121.

(7) Vassilev, S. V.; Baxter, D.; Andersen, L. K.; Vassileva, C. G. An overview of the composition and application of biomass ash.: Part 2. Potential utilisation, technological and ecological advantages and challenges. *Fuel* **2013**, *105*, 19−39.

(8) Voshell, S.; Mäkelä, M.; Dahl, O. A review of biomass ash properties towards treatment and recycling. *Renew. Sustain. Energy Rev.* **2018**, *96*, 479−486.

(9) Ahmaruzzaman, M. A review on the utilization of fly ash. *Prog. Energy Combust. Sci.* **2010**, *36*, 327−363.

(10) Vassilev, S. V.; Vassileva, C. G.; Song, Y.-C.; Li, W.-Y.; Feng, J. Ash contents and ash-forming elements of biomass and their significance for solid biofuel combustion. *Fuel* **2017**, *208*, 377−409.

(11) Onutai, S.; Kobayashi, T.; Thavorniti, P.; Jiemsirilers, S. Porous fly ash-based geopolymer composite fiber as an adsorbent for removal of heavy metal ions from wastewater. *Mater. Lett.* **2019**, *236*, 30−33.

(12) Visa, M.; Bogatu, C.; Duta, A. Tungsten oxide − fly ash oxide composites in adsorption and photocatalysis. *J. Hazard. Mater.* **2015**, *289*, 244−256.

(13) Mushtaq, F.; Zahid, M.; Bhatti, I. A.; Nasir, S.; Hussain, T. Possible applications of coal fly ash in wastewater treatment. *J. Environ. Manage.* **2019**, *240*, 27−46.

(14) Hosseini Asl, S. M.; Javadian, H.; Khavarpour, M.; Belviso, C.; Taghavi, M.; Maghsudi, M. Porous adsorbents derived from coal fly ash as cost-effective and environmentally-friendly sources of aluminosilicate for sequestration of aqueous and gaseous pollutants: A review. *J. Clean. Prod.* **2019**, *208*, 1131−1147.

(15) Thirumalai, K.; Balachandran, S.; Swaminathan, M. Superior photocatalytic, electrocatalytic, and self-cleaning applications of Fly ash supported ZnO nanorods. *Mater. Chem. Phys.* **2016**, *183*, 191−200.

(16) Chen, J.-W.; Yuan, B.; Shi, J.-W.; Yang, J.-C. E.; Fu, M.-L. Reduced graphene oxide and titania nanosheet cowrapped coal fly ash microspheres alternately as a novel photocatalyst for water treatment. *Catal. Today* **2018**, *315*, 247−254.

(17) Mazumder, N. A.; Rano, R. An efficient solid base catalyst from coal combustion fly ash for green synthesis of dibenzylideneacetone. *J. Ind. Eng. Chem.* **2015**, *29*, 359−365.

(18) Fan, H.; Chen, D.; Ai, X.; Han, S.; Wei, M.; Yang, L.; Liu, H.; Yang, J. Mesoporous TiO2 coated ZnFe2O4 nanocomposite loading on activated fly ash cenosphere for visible light photocatalysis. *RSC Adv.* **2018**, *8*, 1398−1406.

(19) Song, J.; Wang, X.; Bu, Y.; Wang, X.; Zhang, J.; Huang, J.; Ma, R.; Zhao, J. Photocatalytic enhancement of floating photocatalyst: Layer-by-layer hybrid carbonized chitosan and Fe-N- codoped TiO2 on fly ash cenospheres. *Appl. Surf. Sci.* **2017**, *391*, 236−250.

(20) Dindi, A.; Quang, D. V.; Vega, L. F.; Nashef, E.; Abu-Zahra, M. R. M. Applications of fly ash for CO2 capture, utilization, and storage. *J. CO2 Util.* **2019**, *29*, 82−102.

(21) Tosti, L.; van Zomeren, A.; Pels, J. R.; Dijkstra, J. J.; Comans, R. N. J. Assessment of biomass ash applications in soil and cement mortars. *Chemosphere* **2019**, *223*, 425−437.
(22) Berra, M.; Mangialardi, T.; Paolini, A. E. Reuse of woody biomass fly ash in cement-based materials. *Constr. Build. Mater.* **2015**, *76*, 286−296.
(23) Nagrockienė, D.; Daugėla, A. Investigation into the properties of concrete modified with biomass combustion fly ash. *Constr. Build. Mater.* **2018**, *174*, 369−375.
(24) Novais, R. M.; Carvalheiras, J.; Senff, L.; Labrincha, J. A. Upcycling unexplored dregs and biomass fly ash from the paper and pulp industry in the production of eco-friendly geopolymer mortars: A preliminary assessment. *Constr. Build. Mater.* **2018**, *184*, 464−472.
(25) Saeli, M.; Tobaldi, D. M.; Seabra, M. P.; Labrincha, J. A. Mix design and mechanical performance of geopolymeric binders and mortars using biomass fly ash and alkaline effluent from paper-pulp industry. *J. Clean. Prod.* **2019**, *208*, 1188−1197.
(26) Bicer, A. Effect of fly ash particle size on thermal and mechanical properties of fly ash-cement composites. *Therm. Sci. Eng. Prog.* **2018**, *8*, 78−82.
(27) Guo, Y.; Zhao, C.; Chen, X.; Li, C. CO2 capture and sorbent regeneration performances of some wood ash materials. *Appl. Energy* **2015**, *137*, 26−36.
(28) López, R.; Díaz, M. J.; González-Pérez, J. A. Extra CO2 sequestration following reutilization of biomass ash. *Sci. Total Environ.* **2018**, *625*, 1013−1020.
(29) Fernández-Delgado Juárez, M.; Mostbauer, P.; Knapp, A.; Müller, W.; Tertsch, S.; Bockreis, A.; Insam, H. Biogas purification with biomass ash. *Waste Manag.* **2018**, *71*, 224−232.
(30) Gao, W.; Fatehi, P. Fly ash based adsorbent for treating bleaching effluent of kraft pulping process. *Sep. Purif. Technol.* **2018**, *195*, 60−69.
(31) Novais, R. M.; Carvalheiras, J.; Tobaldi, D. M.; Seabra, M. P.; Pullar, R. C.; Labrincha, J. A. Synthesis of porous biomass fly ash-based geopolymer spheres for efficient removal of methylene blue from wastewaters. *J. Clean. Prod.* **2019**, *207*, 350−362.
(32) Novais, R. M.; Ascensão, G.; Tobaldi, D. M.; Seabra, M. P.; Labrincha, J. A. Biomass fly ash geopolymer monoliths for effective methylene blue removal from wastewaters. *J. Clean. Prod.* **2018**, *171*, 783−794.
(33) Zhao, C.; Guo, Y.; Yan, J.; Sun, J.; Li, W.; Lu, P. Enhanced CO2 sorption capacity of amine-tethered fly ash residues derived from co-firing of coal and biomass blends. *Appl. Energy* **2019**, *242*, 453−461.
(34) Wang, P.; Guo, Y.; Zhao, C.; Yan, J.; Lu, P. Biomass derived wood ash with amine modification for post-combustion CO2 capture. *Appl. Energy* **2017**, *201*, 34−44.
(35) Yameen, B.; Kaltbeitzel, A.; Langner, A.; Duran, H.; Müller, F.; Gösele, U.; Azzaroni, O.; Knoll, W. Facile Large-Scale Fabrication of Proton Conducting Channels. *J. Am. Chem. Soc.* **2008**, *130*, 13140−13144.
(36) Yameen, B.; Kaltbeitzel, A.; Langer, A.; Müller, F.; Gösele, U.; Knoll, W.; Azzaroni, O. Highly Proton-Conducting Self-Humidifying Microchannels Generated by Copolymer Brushes on a Scaffold. *Angew. Chem., Int. Ed.* **2009**, *48*, 3124−3128.
(37) Yameen, B.; Kaltbeitzel, A.; Glasser, G.; Langner, A.; Müller, F.; Gösele, U.; Knoll, W.; Azzaroni, O. Hybrid Polymer−Silicon Proton Conducting Membranes via a Pore-Filling Surface-Initiated Polymerization Approach. *ACS Appl. Mater. Interfaces* **2010**, *2*, 279−287.
(38) Kusumastuti, E.; Isnaeni, D.; Sulistyaningsih, T.; Mahatmanti, F. W.; Jumaeri; Atmaja, L.; Widiastuti, N. The Effect of Silane Addition on Chitosan-Fly Ash/CTAB as Electrolyte Membrane. *IOP Conf. Ser.: Mater. Sci. Eng.* **2017**, *172*, 012016.
(39) Feyyisa, J. L.; Daniels, J. L.; Pando, M. A.; Ogunro, V. O. Relationship between breakthrough pressure and contact angle for organo-silane treated coal fly ash. *Environ. Technol. Innovat.* **2019**, *14*, 100332.
(40) Sroka, J.; Rybak, A.; Sekula, R.; Filipczak, P.; Kozanecki, M.; Sitarz, M. Two-Step Procedure of Fly Ash Modification as an Alternative Method for Creation of Functional Composite. *J. Polym. Environ.* **2017**, *25*, 1342−1347.
(41) Cui, Z.; Liu, J.; Gao, H.; Xue, Y.; Hao, J.; Zhang, R.; Ji, B.; Chen, J. Size and shape dependences of the adsorption kinetics of malachite green on nano-MgO: a theoretical and experimental study. *Phys. Chem. Chem. Phys.* **2019**, *21*, 13721−13729.
(42) Butt, A.; Farrukh, A.; Ghaffar, A.; Duran, H.; Oluz, Z.; ur Rehman, H.; Hussain, T.; Ahmad, R.; Tahir, A.; Yameen, B. Design of enzyme-immobilized polymer brush-grafted magnetic nanoparticles for efficient nematicidal activity. *RSC Adv.* **2015**, *5*, 77682−77688.
(43) Farrukh, A.; Akram, A.; Ghaffar, A.; Hanif, S.; Hamid, A.; Duran, H.; Yameen, B. Design of Polymer-Brush-Grafted Magnetic Nanoparticles for Highly Efficient Water Remediation. *ACS Appl. Mater. Interfaces* **2013**, *5*, 3784−3793.
(44) Sharma, R.; Kamal, A.; Mahajan, R. K. A quantitative appraisal of the binding interactions between an anionic dye, Alizarin Red S, and alkyloxypyridinium surfactants: a detailed micellization, spectroscopic and electrochemical study. *Soft Matter* **2016**, *12*, 1736−1749.
(45) Moriguchi, T.; Yano, K.; Nakagawa, S.; Kaji, F. Elucidation of adsorption mechanism of bone-staining agent alizarin red S on hydroxyapatite by FT-IR microspectroscopy. *J. Colloid Interface Sci.* **2003**, *260*, 19−25.
(46) Gholivand, M. B.; Yamini, Y.; Dayeni, M.; Seidi, S.; Tahmasebi, E. Adsorptive removal of alizarin red-S and alizarin yellow GG from aqueous solutions using polypyrrole-coated magnetic nanoparticles. *J. Environ. Chem. Eng.* **2015**, *3*, 529−540.
(47) Machado, F. M.; Carmalin, S. A.; Lima, E. C.; Dias, S. L. P.; Prola, L. D. T.; Saucier, C.; Jauris, I. M.; Zanella, I.; Fagan, S. B. Adsorption of Alizarin Red S Dye by Carbon Nanotubes: An Experimental and Theoretical Investigation. *J. Phys. Chem. C* **2016**, *120*, 18296−18306.
(48) Malak, M.; Imen, N.; Yassine, M.; Nebil, S.; Nizar, B. Electrochemical Oxidation of Bromothymol Blue: Application to Textile Industrial Wastewater Treatment. *J. Adv. Oxid. Technol.* **2015**, *18*, 105−113.
(49) Khan, T. A.; Nazir, M. Enhanced adsorptive removal of a model acid dye bromothymol blue from aqueous solution using magnetic chitosan-bamboo sawdust composite: Batch and column studies. *Environ. Prog. Sustain. Energy* **2015**, *34*, 1444−1454.
(50) Lubbad, S. H.; Balsam Kamal Abu, A.-R.; Fawzi Suliman, K. Adsorptive-removal of Bromothymol Blue as Acidic-dye Probe from Water Solution Using Latvian Sphagnum Peat Moss: Thermodynamic Assessment, Kinetic and Isotherm Modeling. *Curr. Green Chem.* **2019**, *6*, 53−61.
(51) Liu, X.; Zhang, S.-Q.; Wei, X.; Yang, T.; Chen, M.-L.; Wang, J.-H. A novel "modularized" optical sensor for pH monitoring in biological matrixes. *Biosens. Bioelectron.* **2018**, *109*, 150−155.
(52) Pathak, A. K.; Bhardwaj, V.; Gangwar, R. K.; De, M.; Singh, V. K. Fabrication and characterization of TiO2 coated cone shaped nano-fiber pH sensor. *Opt. Commun.* **2017**, *386*, 43−48.
(53) Yameen, B.; Ali, M.; Neumann, R.; Ensinger, W.; Knoll, W.; Azzaroni, O. Synthetic Proton-Gated Ion Channels via Single Solid-State Nanochannels Modified with Responsive Polymer Brushes. *Nano Lett.* **2009**, *9*, 2788−2793.
(54) Yameen, B.; Ali, M.; Neumann, R.; Ensinger, W.; Knoll, W.; Azzaroni, O. Single Conical Nanopores Displaying pH-Tunable Rectifying Characteristics. Manipulating Ionic Transport With Zwitterionic Polymer Brushes. *J. Am. Chem. Soc.* **2009**, *131*, 2070−2071.
(55) Yameen, B.; Ali, M.; Neumann, R.; Ensinger, W.; Knoll, W.; Azzaroni, O. Proton-regulated rectified ionic transport through solid-state conical nanopores modified with phosphate-bearing polymer brushes. *Chem. Commun.* **2010**, *46*, 1908−1910.
(56) Hair, M. L.; Hertl, W. Adsorption on hydroxylated silica surfaces. *J. Phys. Chem.* **1969**, *73*, 4269−4276.
(57) Litefti, K.; Freire, M. S.; Stitou, M.; González-Álvarez, J. Adsorption of an anionic dye (Congo red) from aqueous solutions by pine bark. *Sci. Rep.* **2019**, *9*, 16530.

https://dx.doi.org/10.1021/acsomega.0c00889
ACS Omega 2020, 5, 15850−15864

(58) Arshadi, M.; SalimiVahid, F.; Salvacion, J. W. L.; Soleymanzadeh, M. Adsorption studies of methyl orange on an immobilized Mn-nanoparticle: kinetic and thermodynamic. *RSC Adv.* **2014**, *4*, 16005−16017.
(59) Wu, F.-C.; Liu, B.-L.; Wu, K.-T.; Tseng, R.-L. A new linear form analysis of Redlich−Peterson isotherm equation for the adsorptions of dyes. *Chem. Eng. J.* **2010**, *162*, 21−27.
(60) Sun, D.; Zhang, X.; Wu, Y.; Liu, X. Adsorption of anionic dyes from aqueous solution on fly ash. *J. Hazard. Mater.* **2010**, *181*, 335−342.
(61) Murugan, P.; ST, R.; VM, B. Characterization, morphology and stability assessment of low-cost industrial by-product as an adsorbent for the removal of methylene blue from aqueous solution. *Sep. Sci. Technol.* **2020**, *55*, 471−486.
(62) Jawad, A. H.; Malek, N. N. A.; Abdulhameed, A. S.; Razuan, R. Synthesis of Magnetic Chitosan-Fly Ash/Fe3O4 Composite for Adsorption of Reactive Orange 16 Dye: Optimization by Box−Behnken Design. *J. Polym. Environ.* **2020**, *28*, 1068−1082.
(63) Supelano, G. I.; Gómez Cuaspud, J. A.; Moreno-Aldana, L. C.; Ortiz, C.; Trujillo, C. A.; Palacio, C. A.; Parra Vargas, C. A.; Mejía Gómez, J. A. Synthesis of magnetic zeolites from recycled fly ash for adsorption of methylene blue. *Fuel* **2020**, *263*, 116800.
(64) Gao, M.; Ma, Q.; Lin, Q.; Chang, J.; Bao, W.; Ma, H. Combined modification of fly ash with Ca(OH)2/Na2FeO4 and its adsorption of Methyl orange. *Appl. Surf. Sci.* **2015**, *359*, 323−330.
(65) Sonar, S. K.; Niphadkar, P. S.; Mayadevi, S.; Joshi, P. N. Preparation and characterization of porous fly ash/NiFe2O4 composite: Promising adsorbent for the removal of Congo red dye from aqueous solution. *Mater. Chem. Phys.* **2014**, *148*, 371−379.
(66) Novais, R. M.; Ascensão, G.; Tobaldi, D. M.; Seabra, M. P.; Labrincha, J. A. Biomass fly ash geopolymer monoliths for effective methylene blue removal from wastewaters. *J. Clean. Prod.* **2018**, *171*, 783−794.
(67) Vignesh Kumar, T. H.; Sivasankar, V.; Fayoud, N.; Oualid, H. A.; Sundramoorthy, A. K. Synthesis and characterization of coral-like hierarchical MgO incorporated fly ash composite for the effective adsorption of azo dye from aqueous solution. *Appl. Surf. Sci.* **2018**, *449*, 719−728.
(68) Kim, Y.; Kim, C.; Choi, I.; Rengaraj, S.; Yi, J. Arsenic Removal Using Mesoporous Alumina Prepared via a Templating Method. *Environ. Sci. Technol.* **2004**, *38*, 924−931.
(69) Yeom, C.; Kim, Y. Adsorption of ammonia using mesoporous alumina prepared by a templating method. *Environ. Eng. Res.* **2017**, *22*, 401−406.
(70) Bristy, S. S.; Rahman, M. M.; Rahman, M. M.; Alam, M. A.; Karim, M. R.; Ahmad, H. Epoxide functionalized γ-Al2O3/Fe3O4/SiO2 nanocomposite and comparative adsorption behavior of a model reactive azo dye. *Int. J. Appl. Ceram. Technol.* **2019**, *16*, 1239−1252.
(71) Kara, M.; Yuzer, H.; Sabah, E.; Celik, M. S. Adsorption of cobalt from aqueous solutions onto sepiolite. *Water Res.* **2003**, *37*, 224−232.
(72) Khan, T. A.; Dahiya, S.; Khan, E. A. Removal of direct red 81 from aqueous solution by adsorption onto magnesium oxide-coated kaolinite: Isotherm, dynamics and thermodynamic studies. *Environ. Prog. Sustain. Energy* **2017**, *36*, 45−58.
(73) Nassar, M. Y.; Ali, E. I.; Zakaria, E. S. Tunable auto-combustion preparation of TiO 2 nanostructures as efficient adsorbents for the removal of an anionic textile dye. *RSC Adv.* **2017**, *7*, 8034−8050.
(74) Sellaoui, L.; Guedidi, H.; SarraWjihi, S.; Reinert, L.; Knani, S.; Duclaux, L.; Ben Lamine, A. Experimental and theoretical studies of adsorption of ibuprofen on raw and two chemically modified activated carbons: new physicochemical interpretations. *RSC Adv.* **2016**, *6*, 12363−12373.
(75) Liu, Q.-S.; Zheng, T.; Wang, P.; Jiang, J.-P.; Li, N. Adsorption isotherm, kinetic and mechanism studies of some substituted phenols on activated carbon fibers. *Chem. Eng. J.* **2010**, *157*, 348−356.
(76) Rajic, N.; Stojakovic, D.; Jovanovic, M.; Logar, N. Z.; Mazaj, M.; Kaucic, V. Removal of nickel(II) ions from aqueous solutions using the natural clinoptilolite and preparation of nano-NiO on the exhausted clinoptilolite. *Appl. Surf. Sci.* **2010**, *257*, 1524−1532.
(77) Kara, A.; Demirbel, E. Kinetic, Isotherm and Thermodynamic Analysis on Adsorption of Cr(VI) Ions from Aqueous Solutions by Synthesis and Characterization of Magnetic-Poly(divinylbenzene-vinylimidazole) Microbeads. *Water, Air, Soil Pollut.* **2012**, *223*, 2387−2403.
(78) Yin, W.; Li, M.; Hu, T.; Xue, Z.; Yu, J.; Chi, R. Preparation of an Adsorbent Based on Amidoxime and Triazole Modified Waste Cotton Fabrics through an Azide−Alkyne Click Reaction with Excellent Adsorption Performance toward Cu(II). *ACS Sustain. Chem. Eng.* **2019**, *7*, 1944−1955.
(79) Shahriman, M. S.; Mohamad Zain, N. N.; Mohamad, S.; Abdul Manan, N. S.; Yaman, S. M.; Asman, S.; Raoov, M. Polyaniline modified magnetic nanoparticles coated with dicationic ionic liquid for effective removal of rhodamine B (RB) from aqueous solution. *RSC Adv.* **2018**, *8*, 33180−33192.
(80) Qurrat-ul-Ain; Khatoon, J.; Shah, M. R.; Malik, M. I.; Khan, I. A. T.; Khurshid, S.; Naz, R. Convenient pH-responsive removal of Acid Black 1 by green l-histidine/iron oxide magnetic nanoadsorbent from water: performance and mechanistic studies. *RSC Adv.* **2019**, *9*, 2978−2996.
(81) Wang, S.; Wu, H. Environmental-benign utilisation of fly ash as low-cost adsorbents. *J. Hazard. Mater.* **2006**, *136*, 482−501.
(82) Mallakpour, S.; Madani, M. A review of current coupling agents for modification of metal oxide nanoparticles. *Prog. Org. Coat.* **2015**, *86*, 194−207.
(83) Meroni, D.; Lo Presti, L.; Di Liberto, G.; Ceotto, M.; Acres, R. G.; Prince, K. C.; Bellani, R.; Soliveri, G.; Ardizzone, S. A Close Look at the Structure of the TiO(2)-APTES Interface in Hybrid Nanomaterials and Its Degradation Pathway: An Experimental and Theoretical Study. *J. Phys. Chem. C* **2017**, *121*, 430−440.
(84) Nayab, S.; Farrukh, A.; Oluz, Z.; Tuncel, E.; Tariq, S. R.; Rahman, H. u.; Kirchhoff, K.; Duran, H.; Yameen, B. Design and Fabrication of Branched Polyamine Functionalized Mesoporous Silica: An Efficient Absorbent for Water Remediation. *ACS Appl. Mater. Interfaces* **2014**, *6*, 4408−4417.
(85) Nayab, S.; Baig, H.; Ghaffar, A.; Tuncel, E.; Oluz, Z.; Duran, H.; Yameen, B. Silica based inorganic−organic hybrid materials for the adsorptive removal of chromium. *RSC Adv.* **2018**, *8*, 23963−23972.
(86) Farrukh, A.; Akram, A.; Ghaffar, A.; Tuncel, E.; Oluz, Z.; Duran, H.; Rehman, H. u.; Yameen, B. Surface-functionalized silica gel adsorbents for efficient remediation of cationic dyes. *Pure Appl. Chem.* **2014**, *86*, 1177−1188.
(87) Dutta, D. P.; Venugopalan, R.; Chopade, S. Manipulating Carbon Nanotubes for Efficient Removal of Both Cationic and Anionic Dyes from Wastewater. *ChemistrySelect* **2017**, *2*, 3878−3888.
(88) Sharifzade, G.; Asghari, A.; Rajabi, M. Highly effective adsorption of xanthene dyes (rhodamine B and erythrosine B) from aqueous solutions onto lemon citrus peel active carbon: characterization, resolving analysis, optimization and mechanistic studies. *RSC Adv.* **2017**, *7*, 5362−5371.

https://dx.doi.org/10.1021/acsomega.0c00889
ACS Omega 2020, 5, 15850−15864